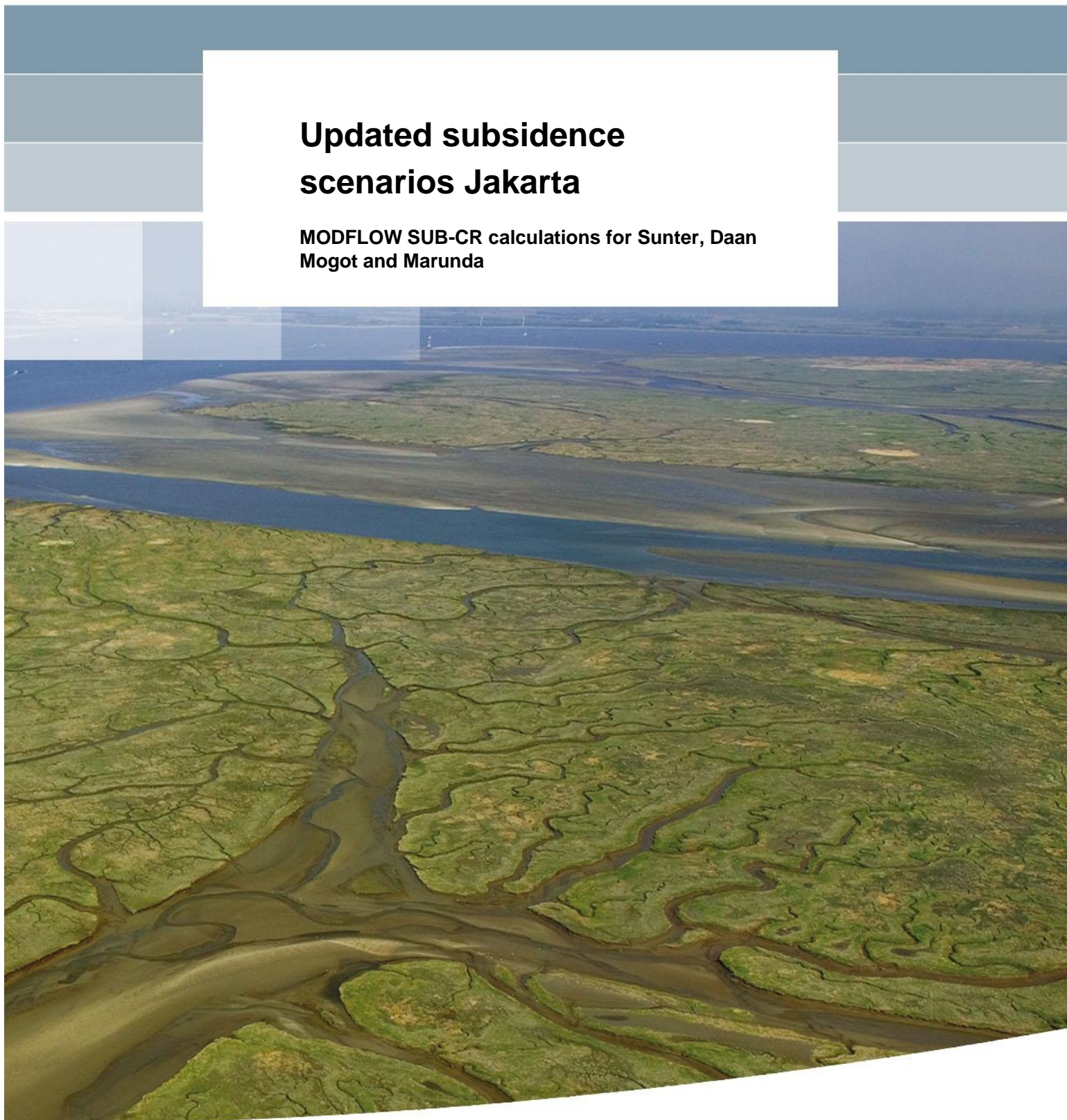# Deltares
Enabling Delta Life

Updated subsidence scenarios Jakarta

MODFLOW SUB-CR calculations for Sunter, Daan Mogot and Marunda

Updated subsidence Scenarios Jakarta

MODFLOW SUB-CR calculations for Sunter, Daan Mogot and Marunda

Henk Kooi
Angga Trysa Yuherdha

11202275-008

Deltares

Title
Updated subsidence scenarios
Jakarta

Client	Project	Reference	Pages
Deltares	11202275-008	11202275-008-BGS-0004	42

Keywords
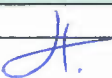Land subsidence; groundwater use; Jakarta; modelling; SUB-CR

Summary
Since 2015 modelling is conducted to provide forecasts of the subsidence that should be anticipated at three locations in northern Jakarta (Daan Mogot, Sunter, Marunda) under different scenarios of groundwater use. The resulting subsidence scenarios are essential for the planning of the integrated measures to protect the city against marine and riverine flooding.
This report provides an update of prior work. The main objective of the work was to shed light on the confidence level of the prognoses. The update includes amongst others:

- A fast and a slow head recovery scenario. This illustrates the range of possible subsidence responses that can occur after groundwater extraction is stopped given the rather large uncertainty of the way in which head recovery will occur.
- Multiple (> 10) subsidence prognoses for each drawdown scenario. This quantifies the sensitivity of the subsidence prognoses for uncertainties regarding the geotechnical and hydraulic property values of the clay-rich layers.
- Elaborate documentation of assumptions, methods, models and parameters.

Calculations were done using MODFLOW in combination with the Deltares-developed SUB-CR package. Results that are presented in tables and figures are of value to set realistic bounds (upper and lower limits) to the subsidence scenarios. This is important for both flood defence measures and subsidence monitoring. The results confirm the conclusion of prior work that it may take up to about two decades for groundwater-extraction-induced subsidence to stop after groundwater extraction stops. The analysis also shows that the uncertainty in this prognosis is large.

Version	Date	Author	Initials	Review	Initials	Approval	Initials
	Aug. 2018	Henk Kooi		Ger de Lange		Henriette Otter	
		Angga Trysa Yuherdha					

State
final

Contents

Appendices

1 Introduction

1.1 Previous work

Land subsidence prognoses for northern Jakarta are essential for the planning of the integrated measures to protect the city against marine and riverine flooding. Extraction of 'deep' groundwater is considered the prime cause of the subsidence that has occurred since the mid 1970's in Jakarta (up to about 4 m). This is indicated by various types of observations, modelling, and experience from many other places in the world. Since 2015 Deltares and PusAir (The water institute of Indonesia in Bandung) are developing modelling-based subsidence forecasts that first seek to explain the past subsidence and then are extended to predict future development for three groundwater-use development scenarios:

1   business as usual (continued lowering of groundwater heads)

2   reduced/controlled deep groundwater use (stabilized groundwater heads)

3   stopped deep groundwater use (recovery of hydraulic heads)

In 2015 first prognoses were made for three locations in western (Daan Mogot), central (Sunter) and eastern (Marunda) parts of north Jakarta (Deltares 2015). June 2017 these prognoses were partly updated using improved subsidence reconstructions provided by ITB for the three locations and limited new hydraulic head data (NCICD 2017). The update focused on the question if subsidence can be stopped in 2028 which served as a basic premise in the updated Master Plan (UMP 2016).

1.2 Present update

In this report a further update of the prognoses is presented. Improvements include:

• Parameterization that is in better agreement with available geotechnical data.
• Use of improved insight in appropriate parameter combinations that avoid previously undetected spurious effects of excessive creep rates.
• More realistic drawdown (and recovery) scenarios.
• An assessment of the confidence level of the subsidence scenarios.

Deltares

2 Methods

2.1 Software

The simulations were done with the SUB-CR land subsidence package of MODFLOW (Deltares 2017). This package was developed by Deltares in recent years and provides an extension with creep (more generally known as secondary consolidation) of the existing SUB-WT land subsidence package of the US Geological Survey. Use of this code overcomes some limitations of the geotechnical code DSettlement that was used in generating the existing/previous prognoses. The employed compression models of DSettlement and SUB-CR are identical (Bjerrum; 4A). However, groundwater conditions can be better represented with MODFLOW SUB-CR. Advantages of SUB-CR for the present application in Jakarta include: (1) the possibility to extend the modelling to regional spatial domains; present modelling is 1D; (2) representation of an impermeable bottom boundary (basement rock).

2.2 1-dimensional calculations

Figure 2.1 illustrates general aspects of the modelling approach.
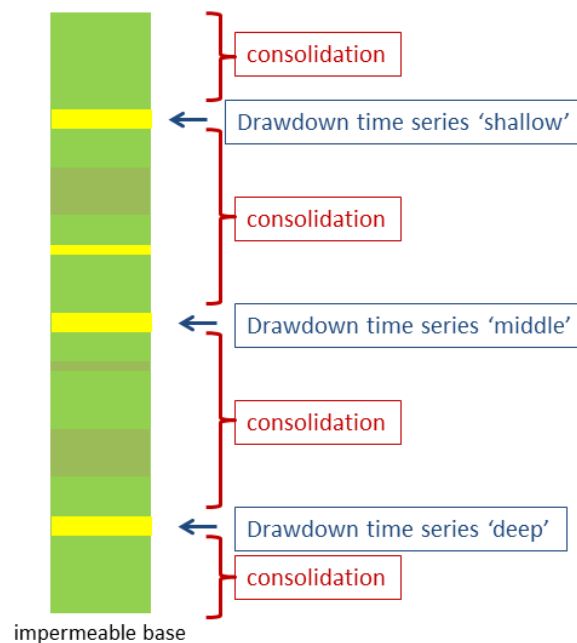
Figure 2.1   Schematic illustration of general aspects of the modelling approach for each site. Drawdown (hydraulic head decline) time series are imposed in sandy units at three depth levels. The lowered pore pressures in these 'pumped' sands induce vertical drainage of the other units (mostly clay-rich) to the 'pumped' levels and the ensuing compression of these layers (consolidation). Head at the top is fixed (at land level). The layer colours indicate use of three different litho-classes.

The key advantage of the 1-dimensional modelling approach is that it allows direct use of observed drawdown data. This avoids having to calibrate the head development at the

various depth levels at the study site by implementing pumping wells with individual pumping regimes in a 3-dimensional representation of the subsurface in the face of inadequate information on these parameters.

Due to the complexity of subsurface geology in northern Jakarta (sandy units embedded in clay rather than distinct aquifer units) and paucity of data for such a complex system, uncertainties are very large. Modelling of local sites where data is relatively complete is still expected to provide most insight and the most meaningful prognoses at this stage. Subsidence modelling coupled with 3-dimensional groundwater flow simulation – such efforts are undertaken as a parallel track (not reported here) – may provide insight in how subsidence responses may vary spatially due to the complex subsurface conditions.

2.3 Study sites

Figure 2.2 shows the three locations that were selected for the previous and present analysis based on available subsidence, geology and groundwater head data: Daan Mogot (Cengkareng), Sunter and Marunda. The map shows that distances between the three data sources (groundwater well, geological borehole, subsidence benchmark) vary up to more than 2 km. Although hydraulic head and geological data are expected to provide important indications for conditions at the subsidence benchmark, the actual conditions at the subsidence benchmark may therefore be different to some unknown degree.
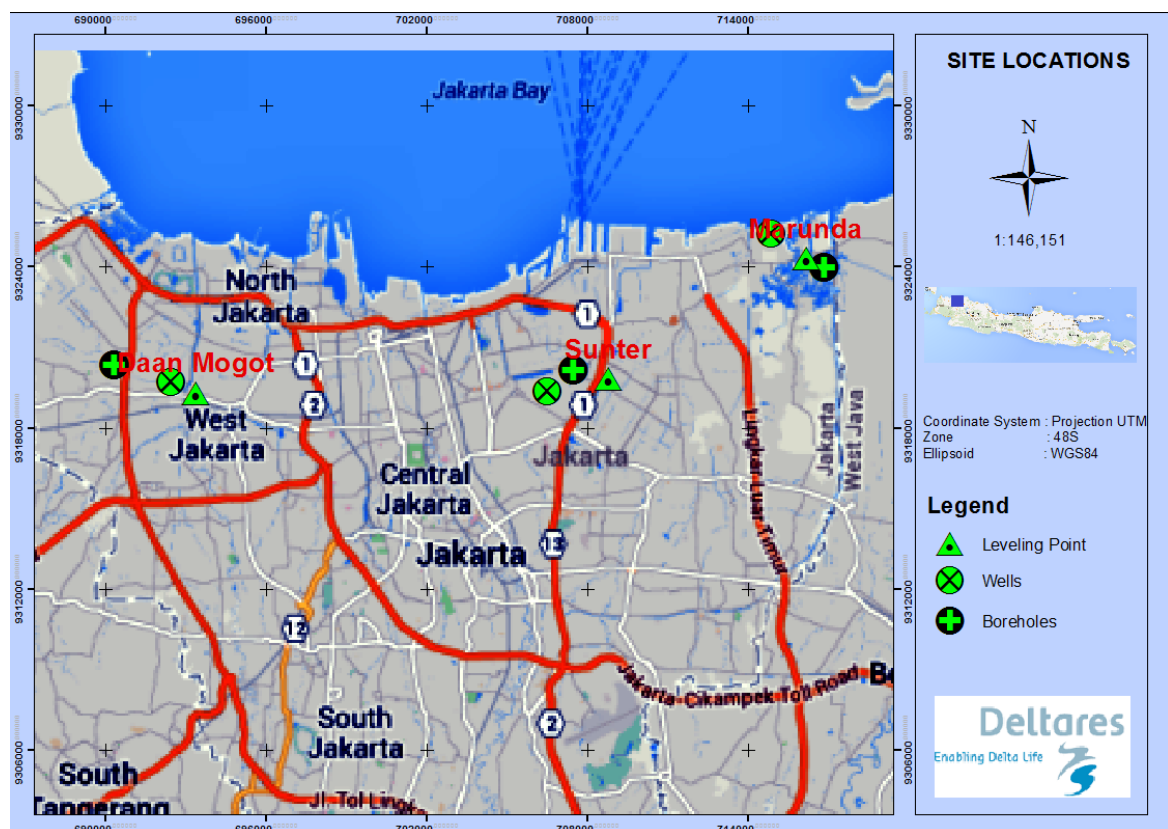

Figure 2.2   The three 'locations' for which subsidence scenarios are developed.

2.4 Key model parameters

Key input parameters for the modelling are:

Compression	
$RR = \dfrac{C_r}{1+e_o}$	recompression or swelling ratio [-]
$CR = \dfrac{C_c}{1+e_o}$	compression ratio [-]
C_a	coefficient of secondary compression [-]

Drainage / consolidation	
$C_v = \dfrac{K_v \ln(10)\sigma'}{\gamma_w CR}$	Terzaghi's consolidation coefficient [m²/s]

Preconsolidation state	
$OCR = \dfrac{\sigma'_p}{\sigma'}$	Overconsolidation ratio [-]
$POP = \dfrac{\sigma'_p - \sigma'}{\gamma_w}$	Preconsolidation stress offset [m]

e_o initial void ratio [-] (from lab tests)

C_r recompression or swelling index [-]

C_c compression index [-]

K_v vertical hydraulic conductivity [m/s]

σ' effective stress [Pa]

σ_p' preconsolidation stress [Pa]

γ_w specific weight of water [N/m³]

2.5 General steps in modelling

The subsidence modelling for each location comprises the following five steps:

1. A layer model is constructed based on the geological borehole in the vicinity of the benchmark for which the reconstructed subsidence time series is available. Three litho-classes are assigned (sand, clay and silty-clay (this also included sandy clay)). Thick clay or silty-clay units are subdivided in smaller layers, notably adjacent to the 'pumped' sand layers to increase the resolution of the finite difference calculations of head development.
2. Drawdown time series are constructed for the period 1925 – 2025 for the three depth levels (four for Sunter) based on hydraulic head data of a nearby groundwater observation well. These are referred to as the *default* drawdown time series.

3. Geotechnical property scenarios (sets) are defined that cover a large range of different compression (RR, CR, C_a) and consolidation (C_v or K_v) and preconsolidation (OCR or POP) conditions for the three litho-classes (constant values per class). Values for RR, CR, C_v, and OCR are bounded by ranges inferred from available geotechnical laboratory test data (shown in paragraph #). For models that include creep ($C_a > 0$) a-priori checks are done to ensure that the OCR is high enough to avoid unrealistically high creep rates for the predevelopment phase (1925).
4. Subsidence is calculated for each geotechnical property scenario and (if needed) an attempt is made to obtain a fit to the observed subsidence, either by increasing C_v with a factor up to 10, or by modifying the default drawdown time series. This step results in a suite of models with different geotechnical parameters that all fit the observations.
5. All fit models are finally used to forecast future subsidence development after 2025 via calculations in which the head- or drawdown time series are extended for the scenarios mentioned in paragraph 1.1: business as usual, deep groundwater use reduced, deep groundwater use stopped. This step results in a suite of prognosis models that gives an impression of the confidence level of prognosis (bandwidth).

In the overall approach, it implicitly assumed that the 'observed' subsidence reconstructions are accurate and that the subsidence is entirely caused by 'deep' groundwater extraction. If the observed subsidence for one or more of the study sites is partly the result of other processes, this approach implies that the current set of subsidence prognoses may overestimate the effectiveness of the mitigation scenarios (partial mitigation or cessation of pumping) to some extent.

2.6 Geotechnical parameter value bounds

Table 2.1 summarizes the bounding values for the geotechnical parameter values for the clay-rich layers (clay and sandy-clay) that were adopted to define the different geotechnical property sets employed in the modelling. The bounds are based on (1) analysis of geotechnical laboratory test data for the NCICD boreholes for the three sites (4B), (2) general considerations of effects of scale and sampling bias (elucidated below), (3) typical values for the coefficient of secondary compression used in geotechnical modelling in The Netherlands and (4) the choice to include calculations without creep (to illustrate what classical elastoplastic models without creep such as SUB-WT would yield).

Table 2.1   Upper and lower bounds for parameters used in modelling based on lab-test data for local boreholes

parameter	units	low	high
RR	-	0.02	0.03
CR	-	0.11	0.17
C_a	-	0	0.005
C_v (clay)	m^2/s	3e-7	3e-6
C_v (silty clay)	m^2/s	5e-7	5e-6
OCR	-	1.0	1.8

Inspection of Figure B.1, Figure B.4, and Figure B.5 shows that CR values measured on core samples include values up to 0.3 and above. Such high values are also known for relatively thin clay units in Holocene strata in The Netherlands. A considerably lower upper bound (Table 2.1) was adopted in the analysis because, in the model calculations, this parameter represents an "effective" value for all the clay and silty-clay units over the entire borehole depth (about 300 m), including much less compressible units. A higher value than adopted was also considered unrealistic since selection of samples for geotechnical measurements may be biased towards the most clay-rich, highly compressible parts of a core.

Preconsolidation stress values are not available from the lab-test report tables. OCR was therefore investigated using an empirical correlation with undrained shear strength data (4B). Results suggest that appropriate average OCR values for clay-rich strata (between 35 and 75 m depth in Sunter) are between 1.5 and 2.0. Values significantly larger than 1.0 are expected when creep causes progressive increase of preconsolidation stress with time (ageing) and do not require unloading. Although we expect that creep plays an important role in the clay-rich sediments in Jakarta, we also include calculations without creep ($C_a = 0$) for reference. SUB-CR without creep is virtually identical to the U.S. Geological Survey package SUB-WT which employs the classical Terzaghi elastoplastic compression relationship. For these simulations without creep we allow OCR to be as low as 1.0 (which equals $POP = 0$ m).

The geotechnical test report tables for the Jakarta boreholes do not include information to constrain the coefficient of secondary compression C_a. A high bound of 0.005 was chosen. This value is representative for moderately stiff pure clay or sandy clay in The Netherlands. Much higher values up to 0.015 are known, for instance for weak organic clays. Although such high values may locally occur in Jakarta, in the absence of geotechnical evidence, the lower value of 0.005 is considered more appropriate for the clay-rich deposits in Jakarta to depths of about three hundred meters..

The C_v values reported from the laboratory tests (4B) are considered to provide lower bounds for model layers that have a thickness that greatly exceeds the thickness of the test specimens that are used in oedometric tests. Effective C_v values for relatively thick units are generally larger due to the presence of sub-layers with a higher C_v. In the subsidence fitting procedure (calibration), the effective C_v was allowed to exceed the laboratory-based low value with a factor of 10.

2.7 Geotechnical (property) scenarios and model name convention

17 Different scenarios for geotechnical properties were defined and used in the modelling (Table 2.2). These cover a large range of compression conditions and preconsolidation states.

Table 2.2   Geotechnical scenarios (for the clay-rich layers) used in the modelling

Scenario/model	RR	CR	Ca	OCR	POP (m)
SCR01	0.03	0.17	0.005	1.5	-
SCR02	0.03	0.15	0.005	1.6	-
SCR03	0.03	0.13	0.005	1.8	-
SCR04	0.03	0.17	0.002	1.2	-
SCR05	0.03	0.15	0.002	1.25	-
SCR06	0.03	0.13	0.002	1.3	-
SCR07	0.03	0.11	0.002	1.3	-
SCR08	0.03	0.17	0.000	1.1	-
SCR09	0.03	0.15	0.000	1.1	-
SCR10	0.03	0.13	0.000	1.0	-
SCR11	0.03	0.11	0.000	1.0	-
SCR12	0.03	0.17	0.000	-	5
SCR13	0.03	0.15	0.000	-	5
SCR14	0.03	0.13	0.000	-	0
SCR15	0.03	0.11	0.000	-	0
SCR16	0.02	0.11	0.002	1.3	-
SCR17	0.02	0.17	0.002	1.2	-

Table 2.3 gives parameter values that are fixed and default values for parameter values that were used in the fitting/optimization process.

Table 2.3   Fixed and default parameter values

	RR	CR	Ca	OCR	Cv (m2/s)
Sand (fixed)	0.001	0.001	0.000	Inf.	high
Clay (default)	-	-	-	-	$3 \cdot 10^{-7}$
Sandy clay (default)	-	-	-	-	$5 \cdot 10^{-7}$

The following naming convention was used to facilitate recognition of key features of the models after optimization:

Convention: SCRXX_YYcv_ZZ

XX   model/scenario number (Table 2.2)

YY   multiplier applied to the default Cv values (Table 2.3)

ZZ   *md* indicates a modified drawdown time series was used relative to the default set of drawdown scenarios described in paragraph 2.8; the chosen drawdown scenario is not included in the naming convention; *EP* indicates the model is elastoplastic (without creep)

2.8 Drawdown scenarios

In the present work several modifications are made to the drawdown trends that are coupled to the three general groundwater-use scenarios (see paragraph 1.1) relative to those used in previous reports (Deltares, 2015; NCICD 2017). These modifications are the following:

- The start of mitigation-induced changes in the drawdown time-series is 2025. This is now considered the earliest date when piped water will be available throughout northern Jakarta, which is a prerequisite to enforce shut down of industrial deep wells.

- For scenario 1 (business as usual), a drawdown increase of 1 m/yr is maintained for all three depth levels, as in previous calculations. However, this drawdown is continued until 2100. In previous calculations drawdown was stabilized after 2050 (NCICD 2017). This may give the false impression that this is due to a 'natural' limit of drawdown.

- Drawdown is not allowed to exceed the depth of groundwater extraction. This applies in particular to the shallow drawdown time series for scenario 1. In prior work such limit was ignored.

- Head recovery in the pumped aquifer units after cessation of pumping (scenario 3) is modelled to be exponential in character rather than a linear 1 m/yr recovery progression. This more closely matches the true recovery behaviour of groundwater systems which shows that head recovery is relatively fast shortly after cessation of pumping, then progressively slowing down as the recovery proceeds. This is approximated by: $s(t) = s(0) e^{-t/\tau}$ where s denotes drawdown and τ the e-folding timescale (at $t = \tau$ about 2/3 of the drawdown that exists when pumping stops ($t = 0$) has recovered). As recovery can be relatively fast or very slow depending on aquifer conditions that are not well known for the study sites (4C), a fast and slow scenario ($\tau = $ 10 and 50 yr) are used. These are referred to as scenarios 3b and 3a, respectively. Results for an intermediate rate recovery scenario (3c; $\tau = $ 30 yr) are presented in 4D.

2.8.1 Drawdown scenarios and groundwater use

It would be very useful if the drawdown scenarios could be translated into (or be based on) reliable or meaningful quantitative scenarios of groundwater use. Unfortunately, this is not feasible. The precise conditions of groundwater use are clear only for scenario 3 (pumping stopped). Stabilized drawdown (scenario 2) implies that groundwater extraction continues, but at limited rates that cannot be known a-priori and that will strongly vary from place to place and depth. 3D groundwater models can provide indications, but results strongly depend on model assumptions. Stabilized drawdown also is very difficult to realize, in particular in the complex subsurface of northern Jakarta. Only with strict regulations and intensive monitoring such conditions can be approached. A good example is Ho Chi Min City, Vietnam where monitoring infrastructure has been established and groundwater users are obliged to stop pumping when the head at a nearby monitoring well has dropped to a predefined value. The precise groundwater extraction rates that correspond to scenario 1 (continued drawdown) also are not known and will also vary spatially. However, in general it requires a progressive increase in production rates at the specific depths at which the drawdowns are applied.

2.8.2   An extra business as usual scenario with future deeper groundwater extraction

A natural development, in particular for the strongly confined (aquifer) conditions that probably prevail in northern Jakarta, is deeper drilling and pumping from deeper pervious strata. This occurred over the past decades, but, without new regulation, is likely to continue in the future. To illustrate the impact of such a progression, some calculations with an extended (greater depth range) model in which drawdown at about 350 m depth is added to the regular scenario 1 case for Marunda, are presented in Appendix 4E.

3 Results

In this chapter the results of the calculations are presented. For each of the three locations first the geological model (column) is shown and the depth levels at which the drawdown time series are applied are indicated. Then the optimized (fitted) subsidence curves + prognoses for scenarios 1, 2, 3a and 3b are presented. 4D provides additional information including:

- The non-optimized subsidence curves for the base-case geotechnical scenarios SCRXX up to 2025.
- Optimized subsidence scenarios for intermediate rate recovery (scenario 3c; $\tau = 30$ yr).
- Parameter values used in the optimized models.
- Modified drawdown time series used to fit specific models.
- Graphs that illustrate the head development with time in depth profiles for some models.

Error! Reference source not found. illustrates the impact of a special 'business as usual' scenario for Marunda in which new drawdown is added below the presently known deepest drawdown level.

3.1 Daan Mogot

3.1.1 Model design

Figure 3.1 shows the layer design of the model and the depth levels at which the drawdown time series are applied. The left panel shows the corresponding depth levels of the screens of the groundwater observation well.
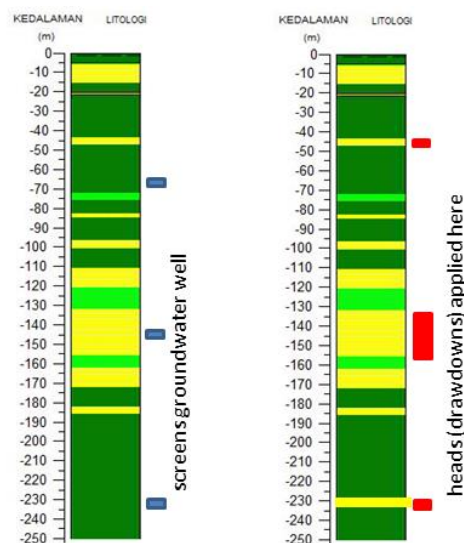

Figure 3.1   Geological column, depth levels of screens of the groundwater observation well (left) and depth levels at which the shallow, middle and deep drawdown time series are applied (right) in the model for the Daan Magot location. Yellow: sand; light green: silty (or sandy) clay; dark green: clay.

3.1.2 Drawdown scenarios

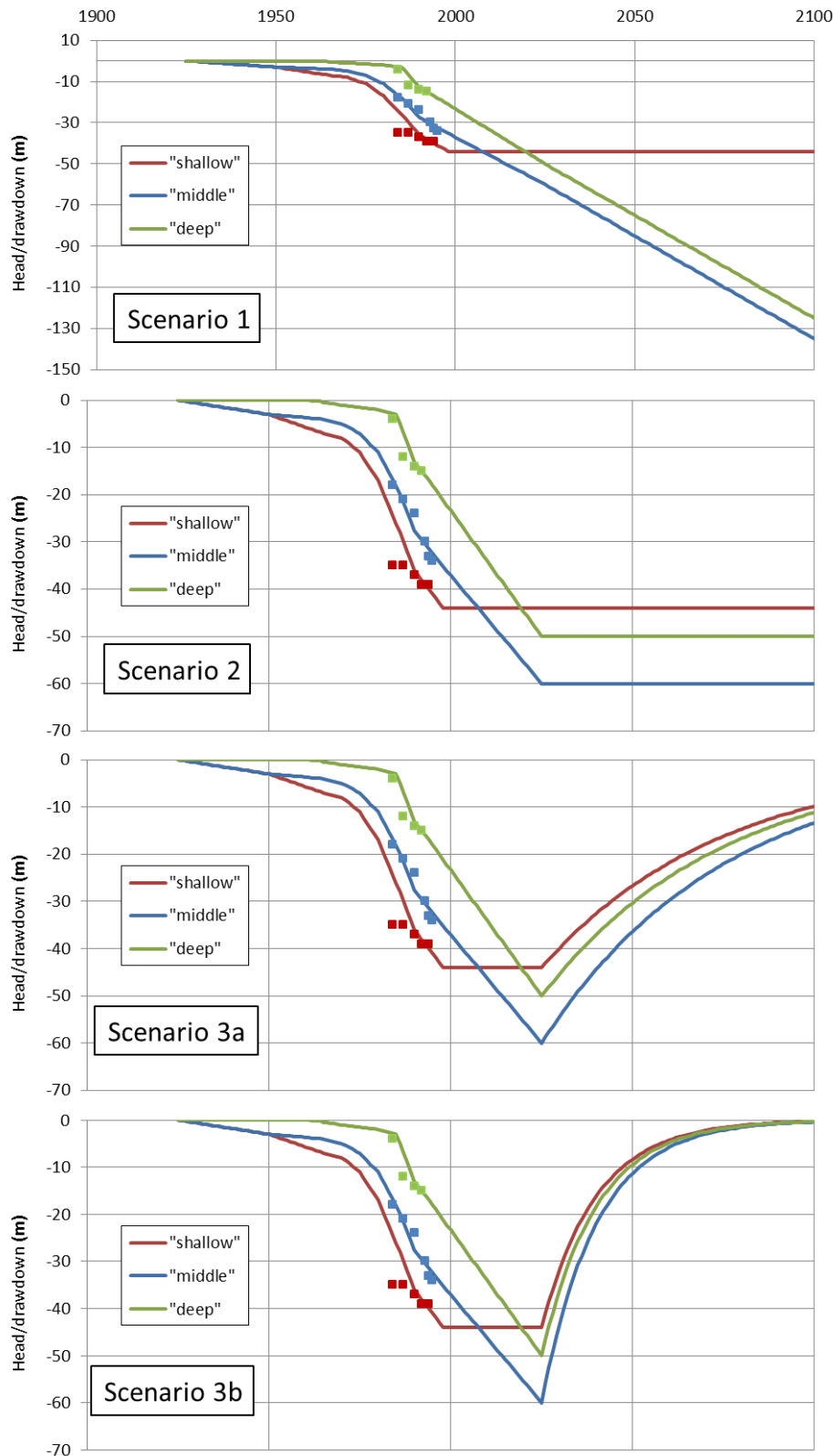*Figure 3.2   Drawdown scenarios for Daan Mogot. The square symbols are observational data with the colour indicating the corresponding well screen.*
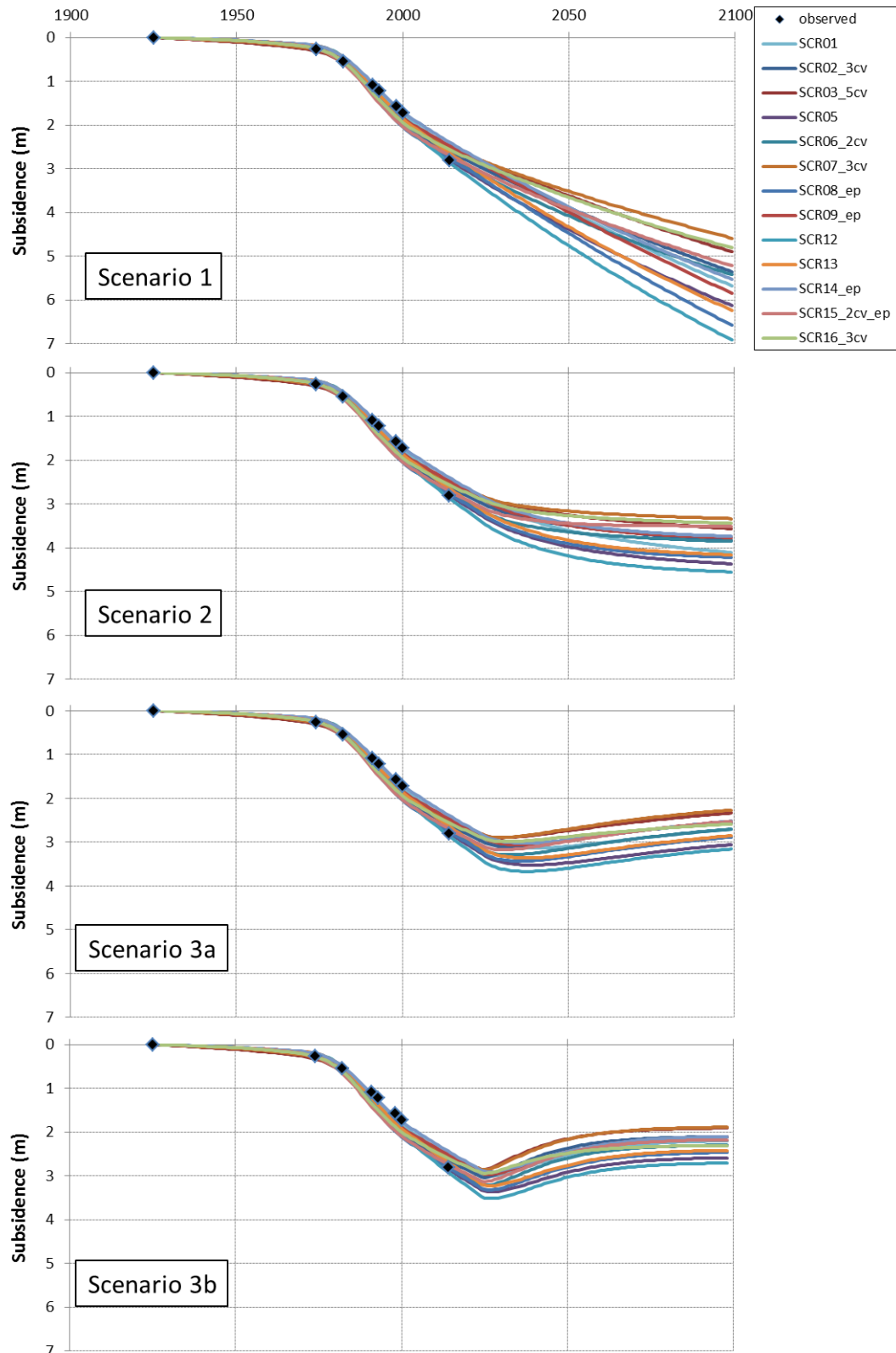
3.1.3 Subsidence scenarios

Figure 3.3   Subsidence scenarios for Daan Mogot.

3.2 Sunter

3.2.1 Model design

Figure 3.4 shows the layer design of the model and the depth levels at which the drawdown time series are applied. The left panel shows the corresponding depth levels of the screens of the groundwater observation well. Drawdown time series corresponding to the three observation well screens are applied at approximately 240, 180 and 90 m depth. Because true 'shallow' groundwater extraction most likely occurs at depths that are considerable less deep than 90 m, a fourth "very shallow" depth level (~ 20 m) was added in the Sunter model. At this extra 'pumping level', $1/7^{th}$ of the drawdown of 90 m depth was applied.
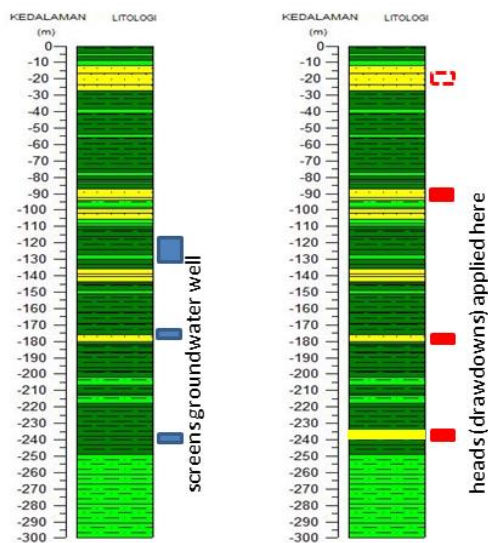

Figure 3.4   Geological column, depth levels of screens of the groundwater observation well (left) and depth levels at which the shallow, middle and deep drawdown time series are applied (right) in the model for the Sunter location. Yellow: sand; light green: silty (or sandy) clay; dark green: clay.
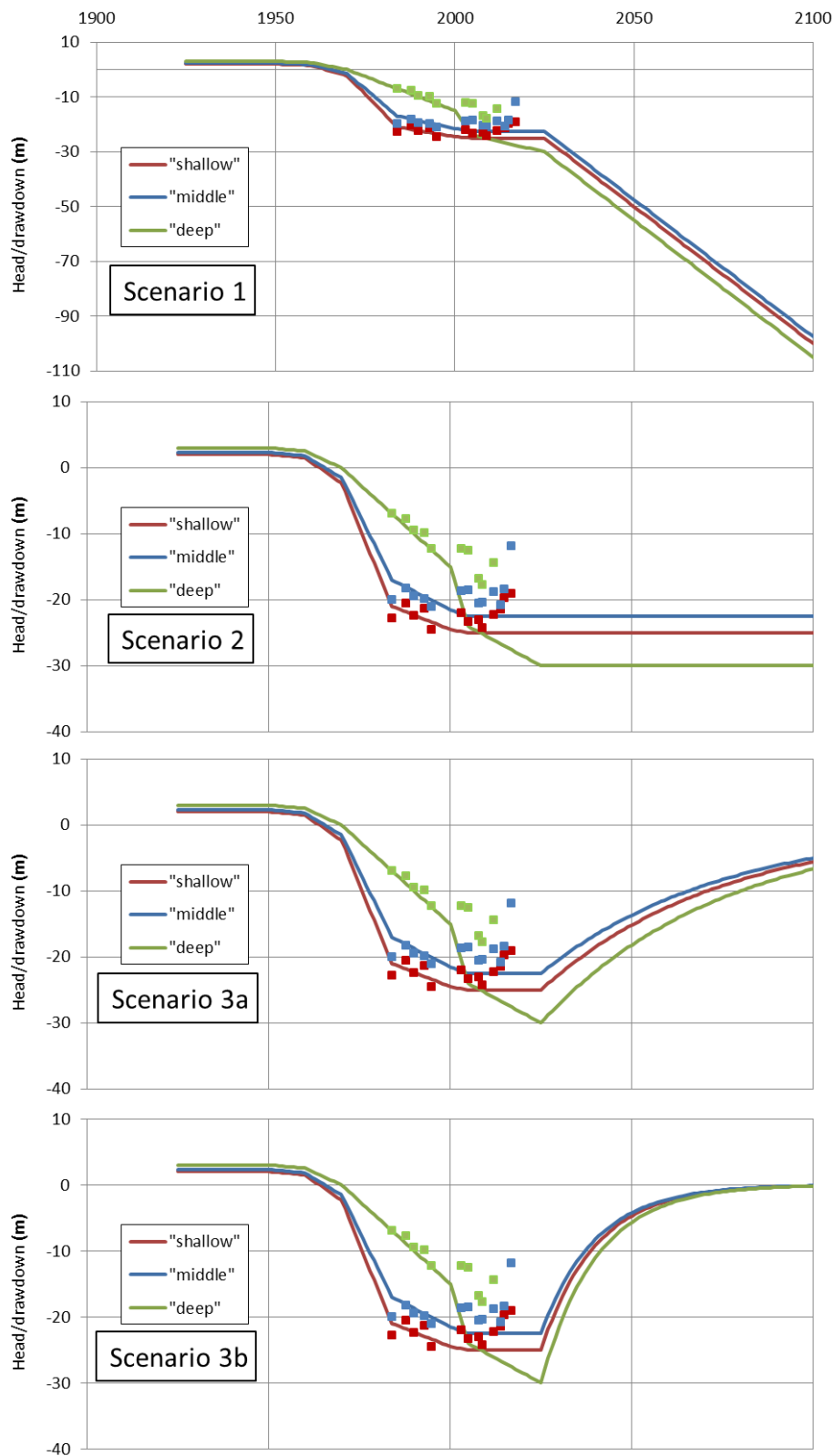
3.2.2   Drawdown scenarios

Figure 3.5   Drawdown scenarios for Sunter. The square symbols are observational data with the colour indicating the corresponding well screen.
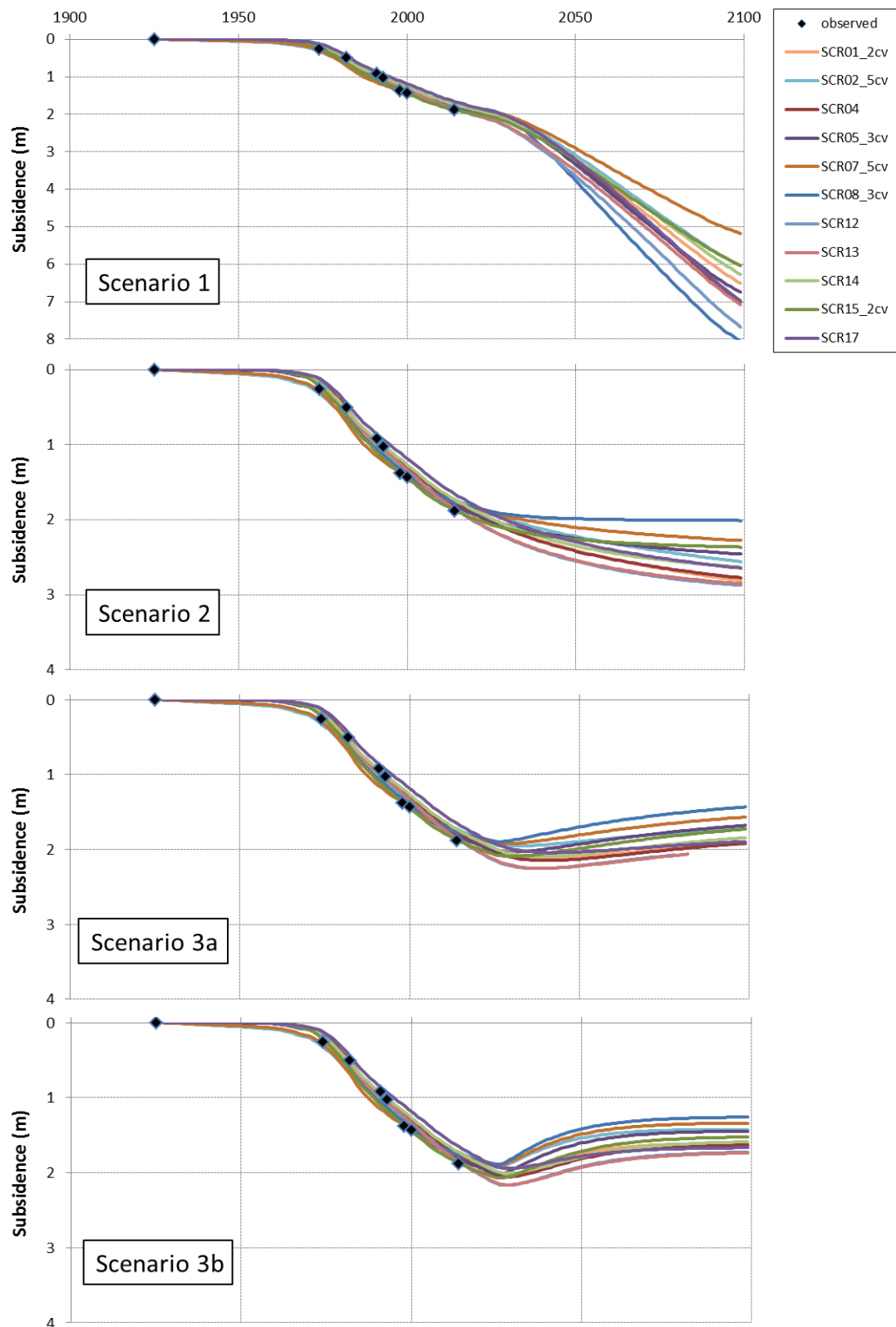
3.2.3 Subsidence scenarios

Figure 3.6 Subsidence scenarios for Sunter.

3.3 Marunda

3.3.1 Model design

Figure 3.7 shows the layer design of the model and the depth levels at which the drawdown time series are applied. The left panel shows the corresponding depth levels of the screens of the groundwater observation well.
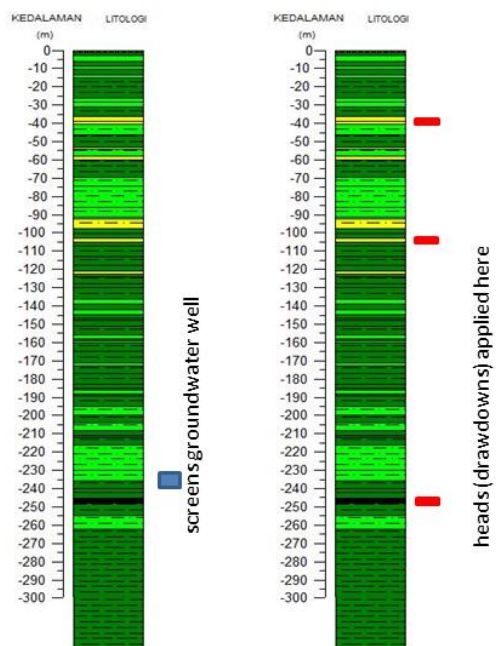

Figure 3.7 Geological column, depth levels of screens of the groundwater observation well (left) and depth levels at which the shallow, middle and deep drawdown time series are applied (right) in the model for the Marunda location. Yellow: sand; light green: silty (or sandy) clay; dark green: clay.

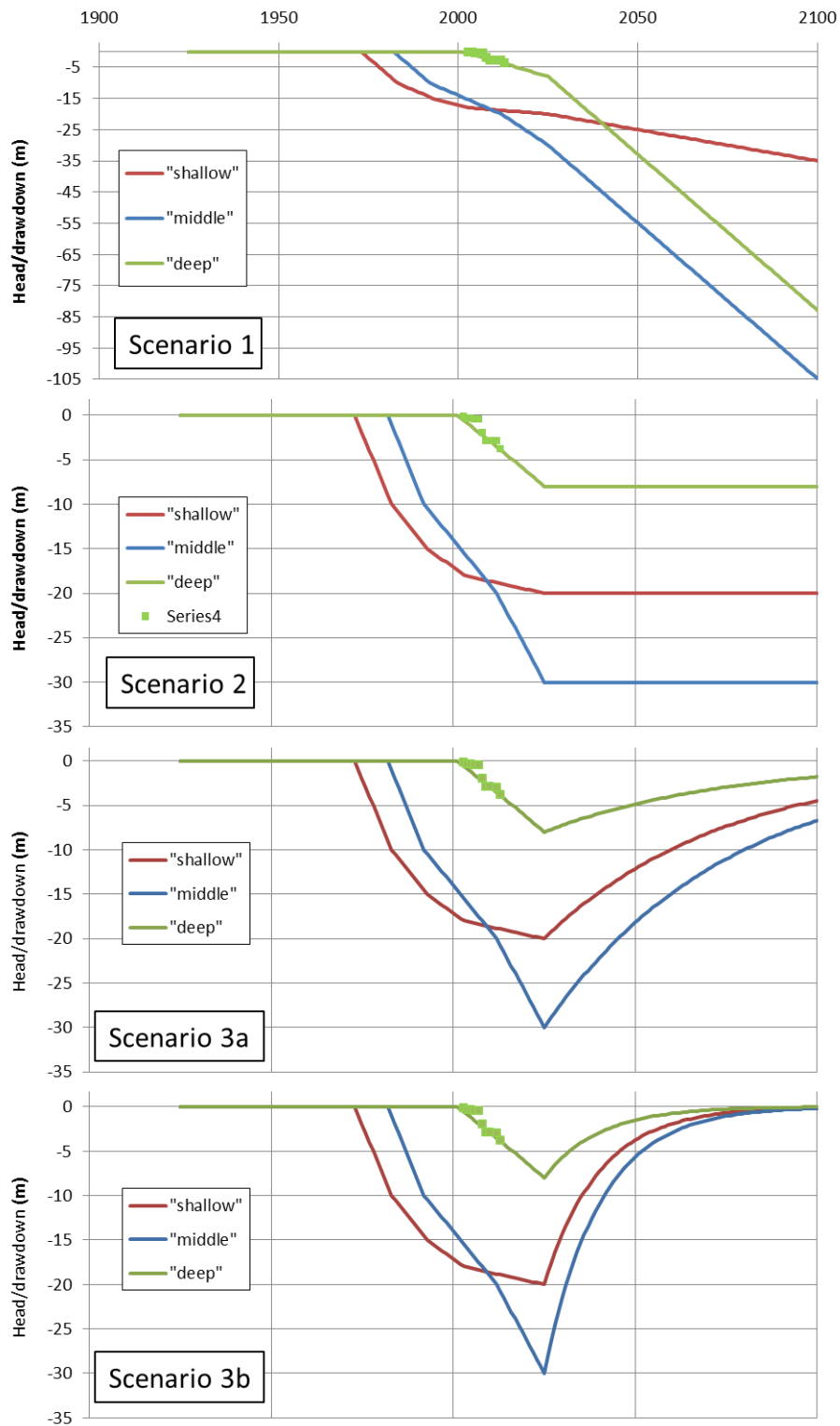## 3.3.2   Drawdown scenarios

*Figure 3.8   Drawdown scenarios for Marunda. A modified drawdown scenario used in one of the models is given in
D.3.3. The square symbols are observational data with the colour indicating the corresponding well screen.*
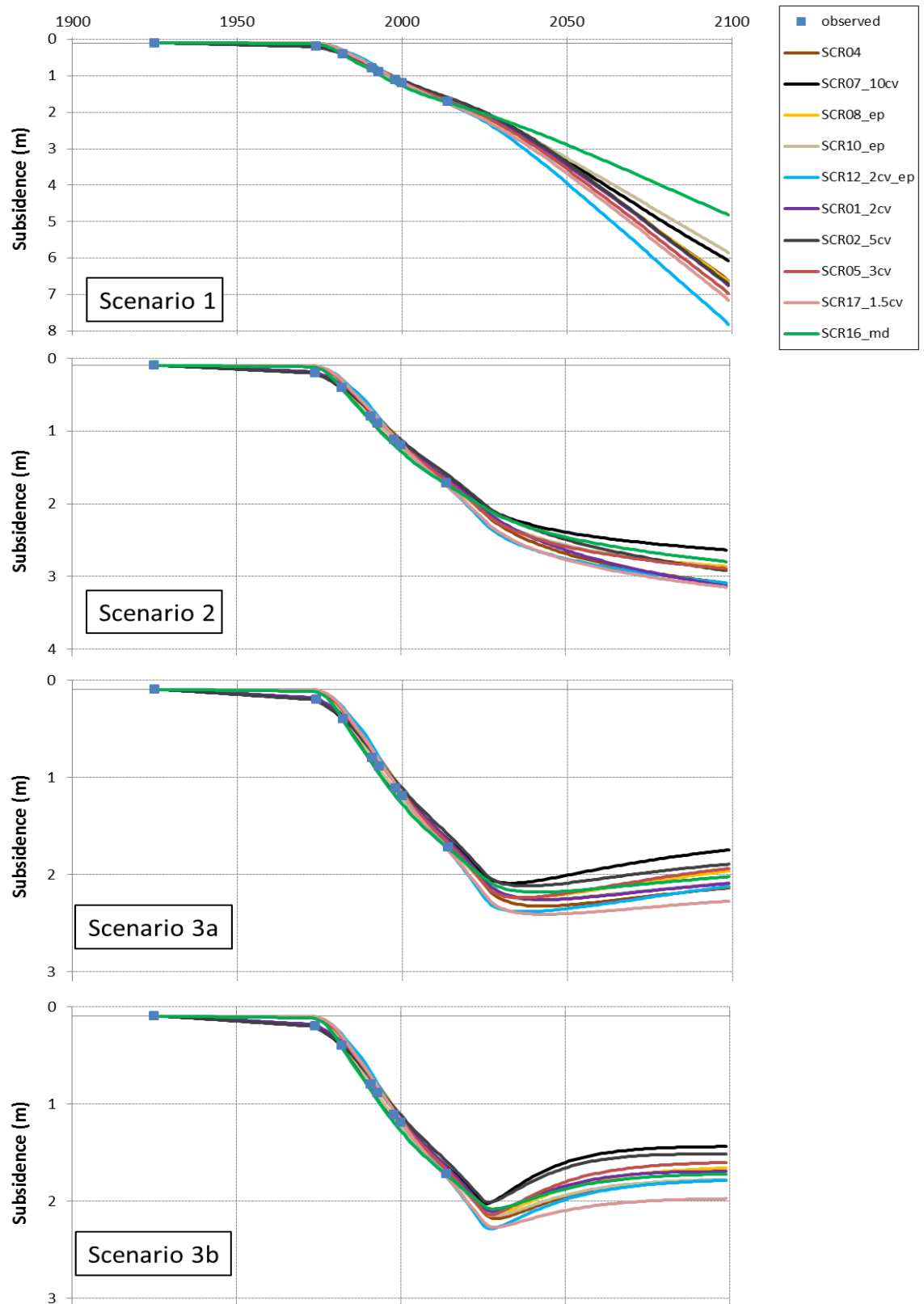
3.3.3 Subsidence scenarios

Figure 3.9   Subsidence scenarios for Marunda.

3.4 Some metrics of the subsidence scenarios

Table 3.1 summarizes predicted subsidence rates in 2018, 2028 and in 2050 for the different scenarios. The table further reports how much subsidence is expected in the periods 2018-2028 and 2018-2050. Minimum and maximum values provide a rough indication of the confidence level (or uncertainty range) of the prognoses.

For the recovery scenarios (3a and 3b), subsidence caused by groundwater use will ultimately stop with some ensuing mild uplift (elastic rebound). Table 3.2 lists how many years of subsidence should be expected after cessation of groundwater extraction in 2025.

Table 3.1   Summary of subsidence and subsidence rates for relevant moments and periods*

	Subsidence rate 2018 (cm/yr)	Subsidence rate 2028 (cm/yr)	Subsidence rate 2050 (cm/yr)	Subsidence 2018-2028 (cm)	Subsidence 2018-2050 (cm)
DAAN MOGOT					
Scenario 1 business as usual	3.2 / 5.6	2.8 / 5.4	2.5 / 4.9	30 / 55	87 / 168
Scenario 2 reduced abstraction	3.2 / 5.6	2.0 / 4.1	0.5 / 1.7	28 / 53	52 / 111
Scenario 3a stopped deep abstraction (slow recovery)	3.2 / 5.6	0.5 / 2.5	-1.2 / -0.7	25 / 49	6 / 52
Scenario 3b stopped deep abstraction (fast recovery)	3.2 / 5.6	-3.0 / 0.1	-2.0 / -1.2	19 / 44	-46 / -3
SUNTER					
Scenario 1 business a.u.	1.3 / 2.7	2.7 / 4.7	5.0 / 9.5	16 / 29	109 / 196
Scenario 2 reduced abstraction	1.3 / 2.7	0.7 / 2.1	0.1 / 1.1	10 / 24	17 / 58
Scenario 3a stopped deep abstraction (slow recovery)	1.3 / 2.7	-0.5 / 1.3	-0.8 / -0.2	8 / 23	-11 / 28
Scenario 3b stopped deep abstraction (fast recovery)	1.3 / 2.7	-2.3 / 0.3	-1.1 / -0.7	4 / 20	-40 / 2
MARUNDA					
Scenario 1 business a.u.	2.8 / 4.4	3.0 / 5.9	3.7 / 7.6	28 / 49	104 / 202
Scenario 2 reduced abstraction	2.8 / 4.4	2.3 / 3.4	0.8 / 1.5	27 / 44	61 / 85
Scenario 3a stopped deep abstraction (slow recovery)	2.8 / 4.4	1.0 / 2.3	-0.7 / -0.2	26 / 41	23 / 48
Scenario 3b stopped deep abstraction (fast recovery)	2.8 / 4.4	-1.6 / 0.5	-1.1 / -0.7	23 / 36	-17 / 18

* reported figures are min. / max. values, respectively

Table 3.2   Years until groundwater-extraction-caused subsidence stops after extraction stops (2025)*

|	DAAN MOGOT	SUNTER	MARUNDA
Scenario 3a (slow recovery)	6 / 15	4 / 18	9 / 19
Scenario 3b (fast recovery)	2 / 5	1 / 5	2 / 5

* reported figures are min. / max. values, respectively

4 References

1 Deltares (2015), Sinking Jakarta, Causes & Remedies, Annex B: Subsidence modelling of the Jakarta alluvial fan-delta.

2 NCICD (2017) Advisory note on Land Subsidence Mitigation.

3 Deltares (2017) Coupled modelling of groundwater flow and land subsidence with creep: MODFLOW/SUB-CR (draft).

A   The Bjerrum compression model

The Bjerrum compression model is a generalization of the classical Terzaghi compression model including secondary compression (creep). Creep is compression that occurs at constant effective stress. This viscous behaviour is evident in laboratory tests of fine-grained sediments as silts and clays as continued log-time continued compression after the phase of primary consolidation has ended (right panel Figure A.1). Compared to Terzaghi, Bjerrum includes one additional compression parameter C_a, the coefficient of secondary compression.

The left panel in Figure A.1 schematically shows the concepts in a log-effective stress versus strain graph. The line separating the light and dark grey zones in the figure is the equivalent of the virgin yield boundary in the Terzaghi compression model. In the Bjerrum model this line is a line of constant creep rate (an isotache). Moving down in the graph creep rates decrease by a factor 10 for each other line (isotache) encountered. C_a represents the creep strain increment between the isotaches.
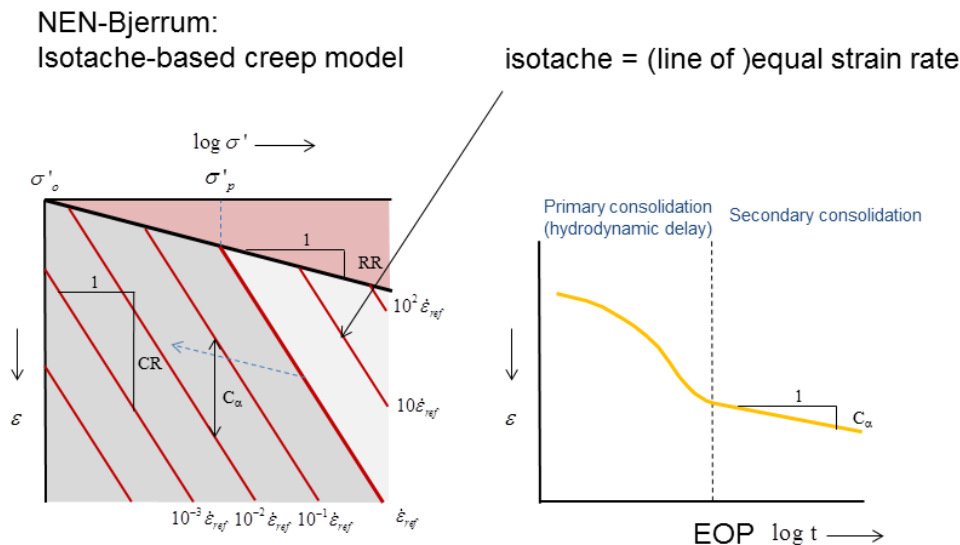
Figure A.1   Graphical representation of the isotache-based creep model after Bjerrum. Left: representation in a stress-strain graph. Right: Secondary compression as the creep phase at constant effective stress following primary consolidation after step loading at t=0.

B Geotechnical parameter values
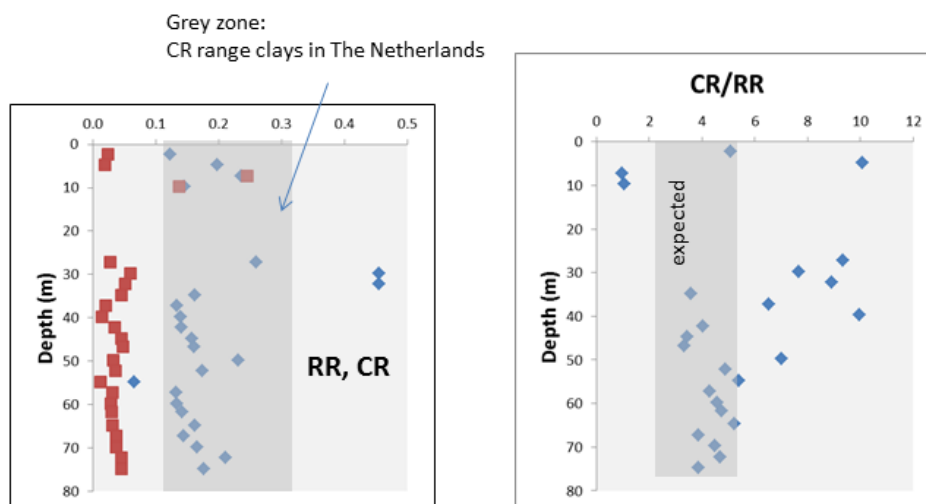
B.1 Sunter

Figure B.1   RR and CR values inferred from geotechnical data for borehole Sunter (from void ratio and compression indices).
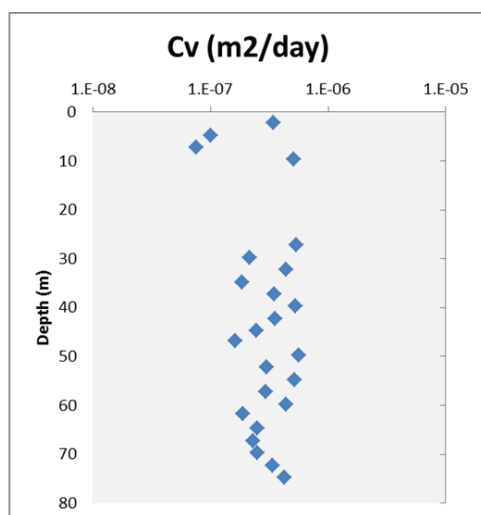

Figure B.2   Cv values for the borehole Sunter

Estimates overconsolidation state of clays from undrained shear strength test (UU) data

Overconsolidation ratio: $OCR = \dfrac{\sigma_p}{\sigma'}$

Significantly > 1, otherwise values remain rather uncertain, Inparticular at greater depth
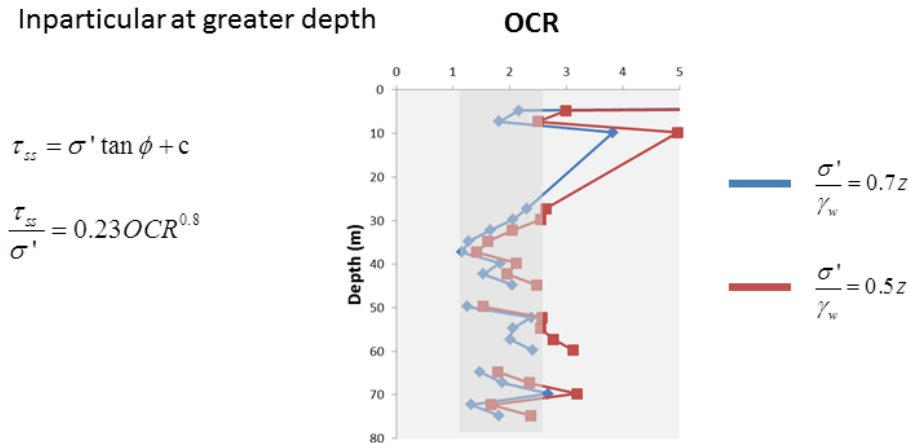
Mayne (2006)
In: Characterization and Engineering properties of natural soils

$\tau_{ss} = \sigma' \tan \phi + c$

$\dfrac{\tau_{ss}}{\sigma'} = 0.23 OCR^{0.8}$

$\dfrac{\sigma'}{\gamma_w} = 0.7z$

$\dfrac{\sigma'}{\gamma_w} = 0.5z$

Figure B.3   OCR value estimates from undrained shear strength data for borehole Sunter.

B.2   Daan Mogot

For the Daan Mogot borehole, estimation of CR from Cc is not as straightforward as for the Sunter and Marunda boreholes because void ratio is not listed in the tabulated data (Maathuis, 1994). For this borehole, void ratio was estimated from $e = m*SG$ where m is moisture content (mass water / mass solids) and *SG* specific gravity (specific weight solids / specific weight water). This assumes water saturation, which is reasonable, except perhaps for the shallowest sample(s). A scan of the original tabulated data (Maathuis, 1994) and a table with calculation results are given below. Figure B.4 CR values inferred from geotechnical data for borehole Daan Mogot (from void ratio estimate and compression indices). shows a graph of the inferred CR values. Similar to the results for the Sunter borehole, CR values are in the range 0.1 – 0.3. Cv values also are consistent with those of Sunter.

Sample Interval	Moisture Content	Specific Gravity	Attenberg Limits				Grain-size distribution				c_c	Average c_v	Average K_v
			LL	PL	PI	LI	Gravel	Sand	Silt	Clay			
m	%		%	%			%	%	%	%		cm²/s	m/s
1.30-1.50	22.66	2.61	75.0	22.2	52.8	0.01	-	10	57	33	0.161	5.25E-03	1.89E-06
5.50-5.20	50.92	2.46	54.5	23.3	31.2	0.89	-	11	77	12	0.413	3.87E-03	2.05E-09
8.10-8.50	52.98	2.46	58.4	20.0	38.4	0.86	-	8	68	24	0.718	2.23E-03	2.05E-09
17.60-17.85	56.37	2.55	77.3	23.4	53.9	0.61	-	9	67	24	0.511	4.76E-03	6.42E-06
20.80-21.00	53.45	2.51	103.5	37.4	66.1	0.24	-	3	54	43	0.347	4.28E-03	1.98E-06
22.10-22.45	38.25	2.51	61.9	22.7	39.3	0.40	-	5	58	37	0.379	3.00E-03	1.61E-09
25.25-25.45	38.05	2.62	86.0	35.1	50.9	0.06	-	2	43	55	0.389	4.57E-03	4.21E-06
27.65-28.00	41.52	2.51	99.0	34.1	64.9	0.11	-	3	52	45	0.414	2.81E-03	1.50E-09
28.50-28.70	39.97	2.58	97.3	28.4	68.8	0.17	-	3	48	49	0.366	4.40E-03	2.69E-06
36.65-36.80	30.20	2.50	80.0	32.0	48.0	-0.04	-	6	54	40	0.254	1.95E-03	9.93E-10
64.00-65.00	33.38	2.66	112.1	28.8	83.4	0.06	-	6	69	25	0.288	1.36E-03	1.76E-09
76.00-77.00	36.17	2.72	115.9	29.3	86.6	0.08	-	3	53	45	0.362	3.07E-03	2.52E-09
85.00-85.50	29.86	2.65	93.0	26.3	66.7	0.05	-	7	44	49	0.463	1.90E-03	2.61E-09
95.00-96.00	35.53	2.65	141.5	32.0	109.5	0.03	-	3	50	47	0.406	2.91E-03	3.17E-09
115.00-116.00	38.93	2.67	130.9	31.9	99.0	0.07	-	6	54	40	0.644	3.23E-03	5.99E-09
155.00-156.00	34.14	2.65	75.9	29.0	46.9	0.11	-	8	56	36	0.360	1.64E-03	1.86E-09
174.00-175.00	38.25	2.71	136.2	29.6	106.6	0.08	-	7	51	42	0.623	1.99E-03	4.08E-09

| Moisture Content %	Specific Gravity							
m reported	SG	top	bottom	middle	m used	e	Cc	CR
22.66	2.61	1.3	1.5	1.4	0.23	0.600	0.161	0.101
50.92	2.46	5.5	5.2	5.35	0.51	1.255	0.413	0.183
52.98	2.46	8.1	8.5	8.3	0.53	1.304	0.718	0.312
56.37	2.55	17.6	17.85	17.725	0.56	1.428	0.511	0.210
53.45	2.51	20.8	21	20.9	0.53	1.330	0.347	0.149
38.25	2.51	22.1	22.45	22.275	0.38	0.954	0.379	0.194
38.05	2.62	25.25	25.45	25.35	0.38	0.996	0.389	0.195
41.52	2.51	27.65	28	27.825	0.42	1.054	0.414	0.202
39.97	2.58	28.5	28.7	28.6	0.40	1.032	0.366	0.180
30.2	2.5	36.65	36.8	36.725	0.30	0.750	0.254	0.145
33.38	2.66	64	65	64.5	0.33	0.878	0.288	0.153
36.17	2.72	76	77	76.5	0.36	0.979	0.362	0.183
29.86	2.65	85	85.5	85.25	0.30	0.795	0.463	0.258
35.53	2.65	95	96	95.5	0.36	0.954	0.406	0.208
38.93	2.67	115	116	115.5	0.39	1.041	0.644	0.315
34.14	2.65	155	156	155.5	0.34	0.901	0.360	0.189
38.25	2.71	174	175	174.5	0.38	1.030	0.623	0.307
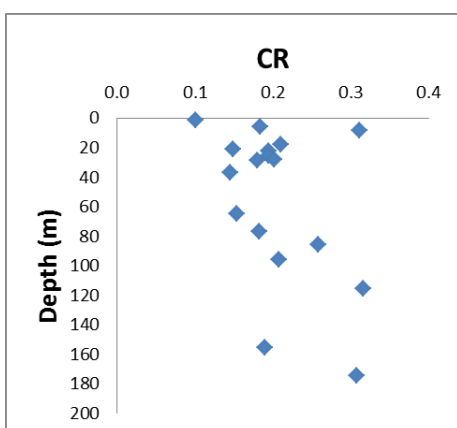
Figure B.4 CR values inferred from geotechnical data for borehole Daan Mogot (from void ratio estimate and compression indices).
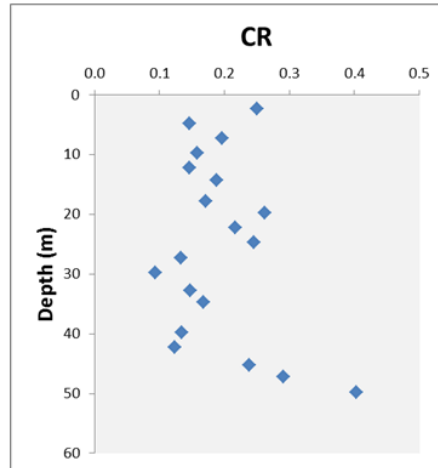
B.3 Marunda

Figure B.5   CR values inferred from geotechnical data for borehole Marunda (from void ratio and compression index).
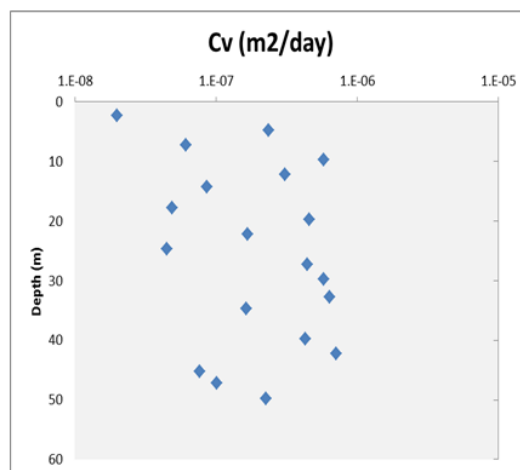

Figure B.6   Cv values inferred from geotechnical data for borehole Marunda.

C   Head recovery rates following cessation of pumping

Numerical modelling was used to investigate plausible head recovery rates for generalized conditions that may occur in northern Jakarta. Calculations were done with FlexPDE (www.pdesolutions.com), a finite-element code for solving of partial differential equations.

The following equation was solved on a 2D domain (cylinder coordinates r, z) extending away from a well bore:

$$S_s \frac{\partial h}{\partial t} = \nabla \cdot \left(\vec{\vec{K}} \nabla h \right)$$

The domain consists of a 5 m thick aquifer overlain by an aquitard. Pumping is represented by a uniform outflow at the wellbore side (screen) of the aquifer ($Q = 500 \, m^3 / day$). The initial head equals the top of the domain which is set to zero. The table below shows the adopted parameter values.

	$K_r \, (m/day)$	$K_z \, (m/day)$	$S_s \, (m^{-1})$
aquitard	$1 \cdot 10^{-3}$	$5 \cdot 10^{-4}$	$5 \cdot 10^{-3}$
aquifer	5	2.5	$1 \cdot 10^{-5}$

Pumping is maintained for 30 years and then stopped. A recovery period of 30 years is modelled. Total simulated time therefore is 60 years.

Three different models are shown here:

Model 1:   laterally extensive aquifer (6 km radial); aquifer at 45-50 m depth
Model 2:   laterally confined aquifer (1 km radial); aquifer at 45-50 m depth
Model 3:   laterally confined aquifer (1 km radial); aquifer at 200-205 m depth
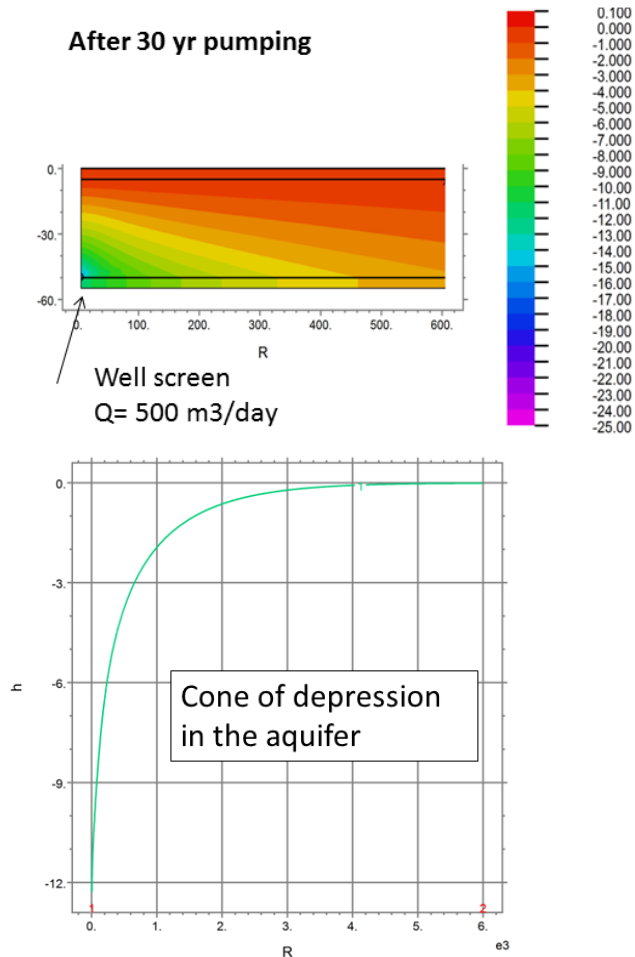
C.1 Model 1

Figure C.1   Model 1. Top: hydraulic head field up to 600 m from the well after 30 years of pumping. Bottom: head profile in the aquifer to 6 km showing the zone of depression (drawdown increasing towards the well).
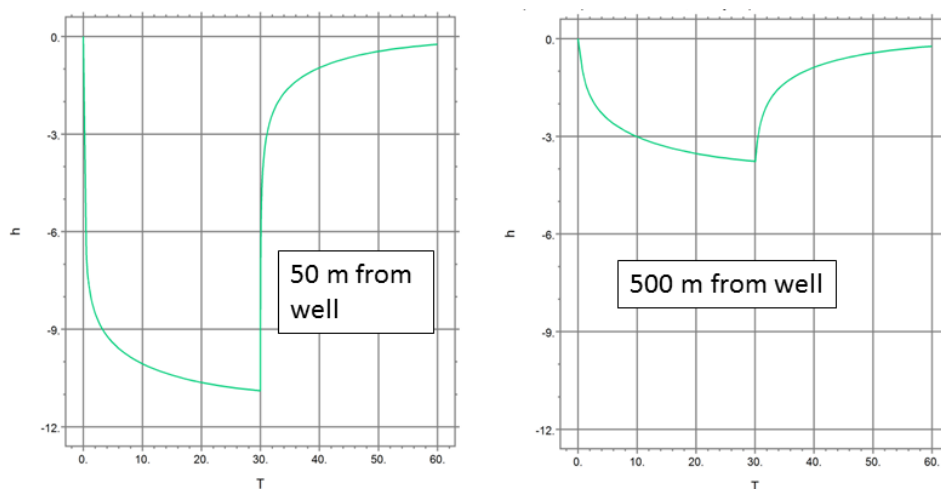

Figure C.2   Model 1: Drawdown and recovery time series in the aquifer at two distances from the well. 2/3 Recovery for the right panel occurs after about 10 years
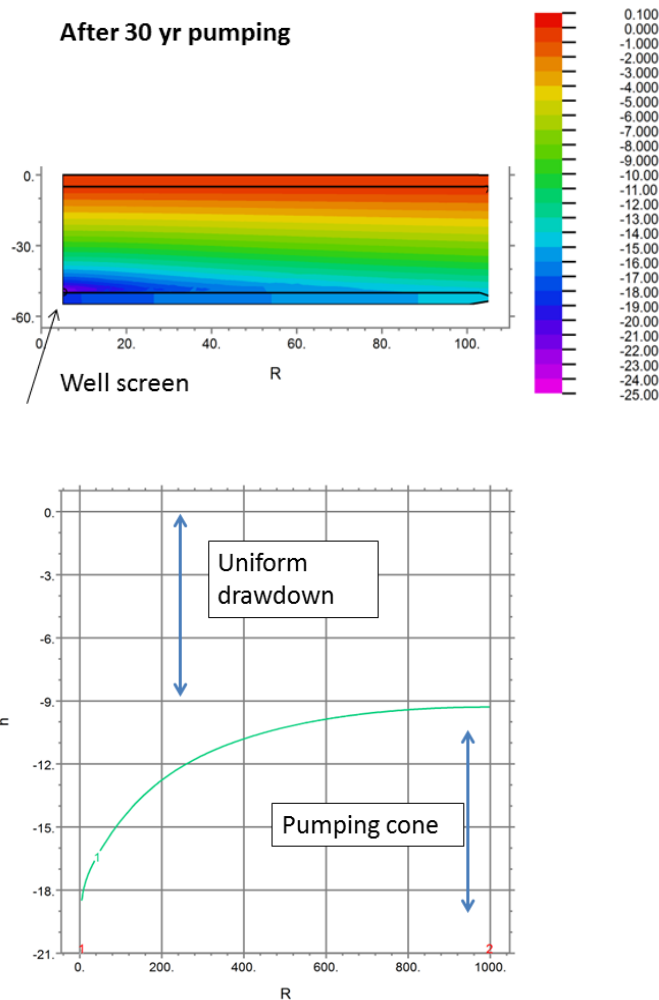
C.2 Model 2

Figure C.3 Model 2. Top: hydraulic head field up to 100 m from the well after 30 years of pumping. Bottom: head profile in the aquifer to 1 km.
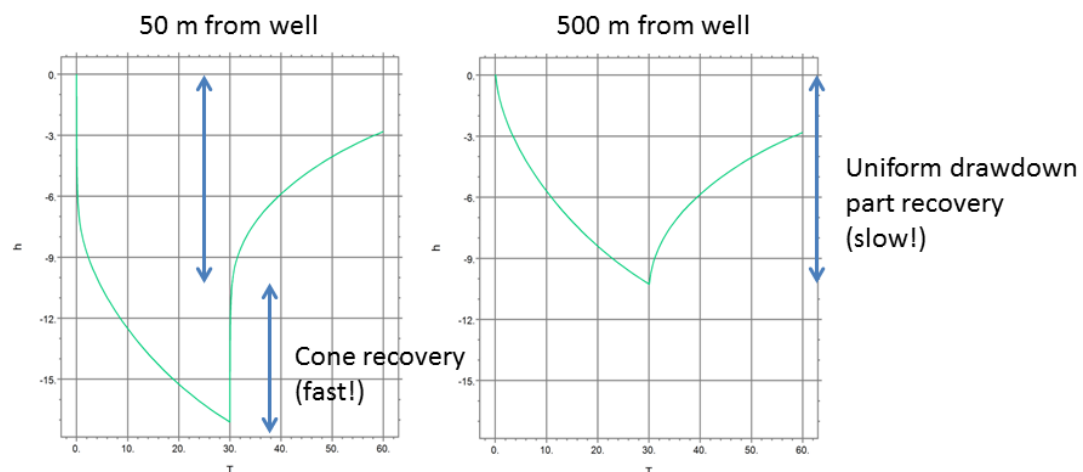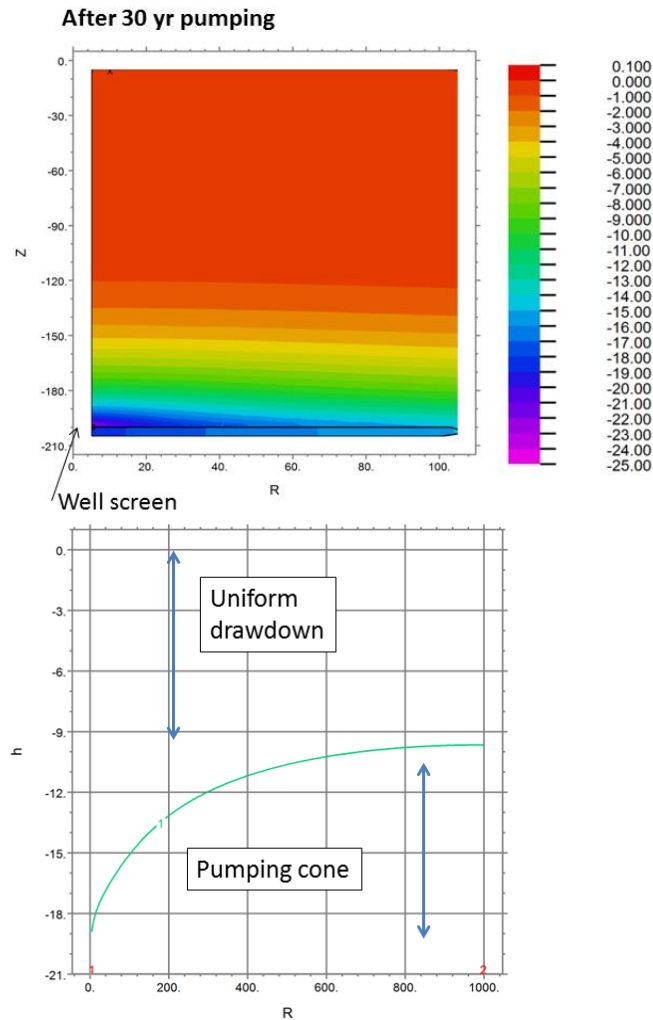

Figure C.4 Model 2: Drawdown and recovery time series in the aquifer at two distances from the well. 2/3 Recovery of the uniform drawdown occurs after about 30 years

C.3 Model 3

After 30 yr pumping

Figure C.5 Model 3. Top: hydraulic head field up to 100 m from the well after 30 years of pumping. Bottom: head profile in the aquifer to 1 km.
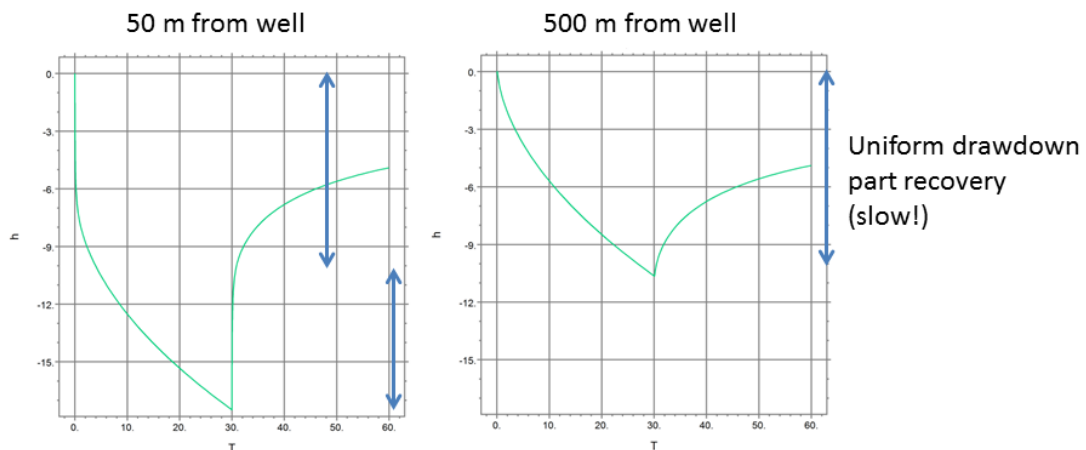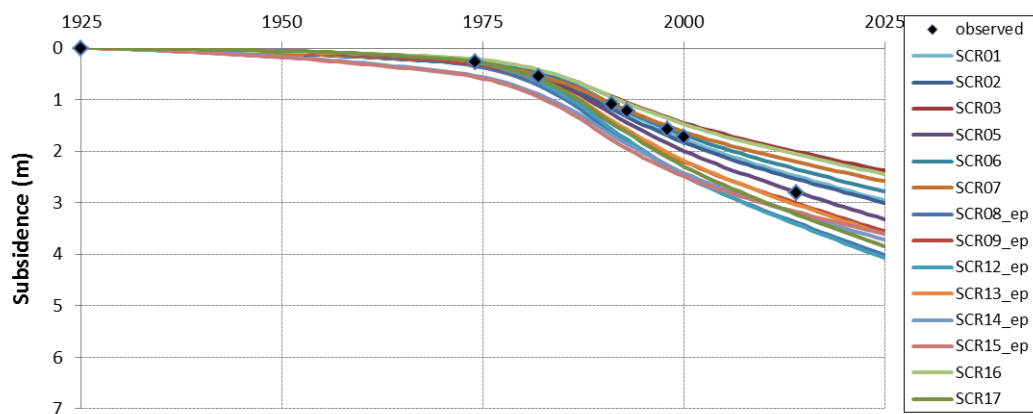

Figure C.6 Model 3: Drawdown and recovery time series in the aquifer at two distances from the well. 2/3 Recovery of the uniform drawdown occurs after about 50 years
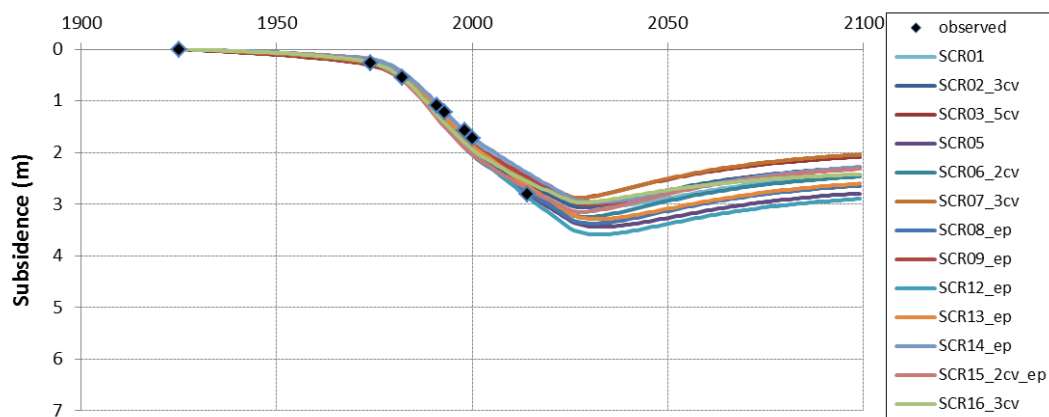
D Additional information regarding model results

D.1 Daan Mogot

D.1.1 Non-optimized subsidence scenarios to 2025.

D.1.2 Intermediate rate recovery ($\tau = 30$ yr)

This scenario (3c) is based on a recovery rate that is intermediate relative to the slow (3a) and fast (3b) scenarios.
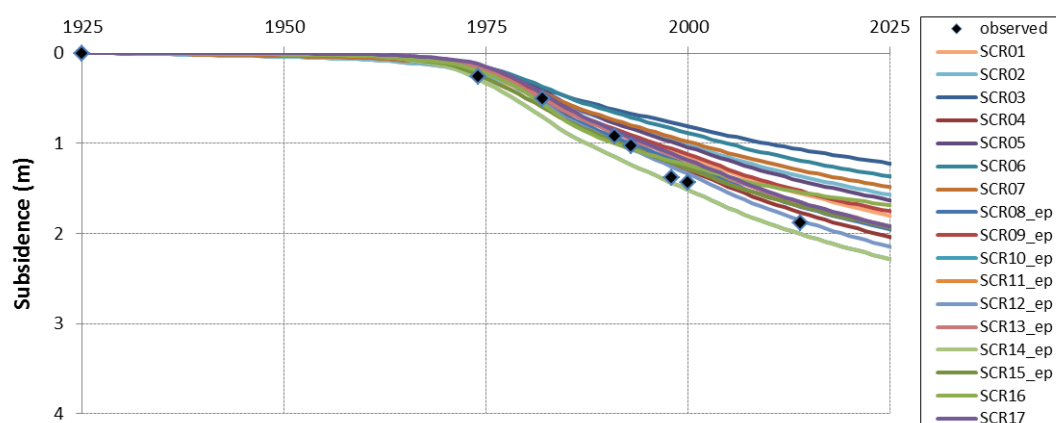
D.1.3   Optimized parameter values

The table shows the optimized OCR and POP values. Optimized Cv values can be inferred from the names shown in the graphs.

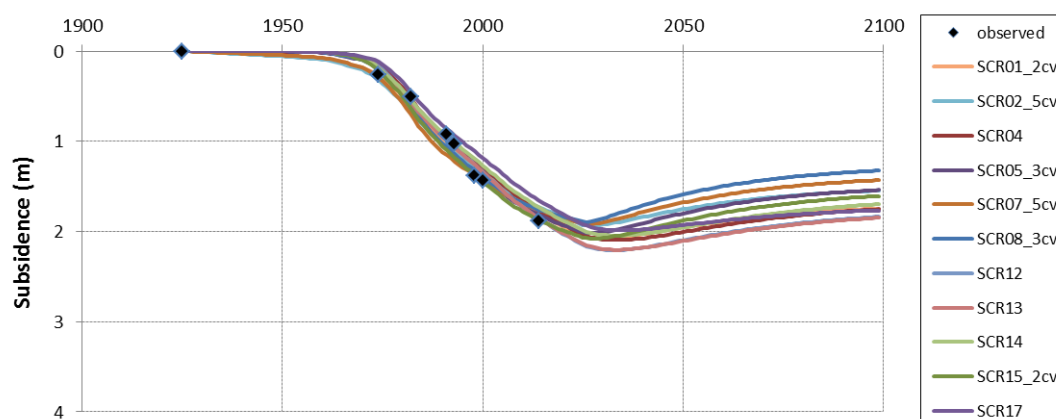| Scenario/model	RR	CR	Ca	OCR	POP (m)
SCR01	0.03	0.17	0.005	**1.6**	-
SCR02	0.03	0.15	0.005	**1.7**	-
SCR03	0.03	0.13	0.005	1.8	-
SCR04	0.03	0.17	0.002	No fit	-
SCR05	0.03	0.15	0.002	1.25	-
SCR06	0.03	0.13	0.002	1.3	-
SCR07	0.03	0.11	0.002	1.3	-
SCR08	0.03	0.17	0.000	**1.2**	-
SCR09	0.03	0.15	0.000	**1.2**	-
SCR10	0.03	0.13	0.000	No fit	-
SCR11	0.03	0.11	0.000	No fit	-
SCR12	0.03	0.17	0.000	-	**10**
SCR13	0.03	0.15	0.000	-	**9**
SCR14	0.03	0.13	0.000	-	**8**
SCR15	0.03	0.11	0.000	-	**5**
SCR16	0.02	0.11	0.002	1.3	-
SCR17	0.02	0.17	0.002	No fit	-

D.2   Sunter

D.2.1   Non-optimized subsidence to 2025.

D.2.2 Intermediate rate recovery ($\tau = 30$ yr)

This scenario (3c) is based on a recovery rate that is intermediate relative to the slow (3a) and fast (3b) scenarios.
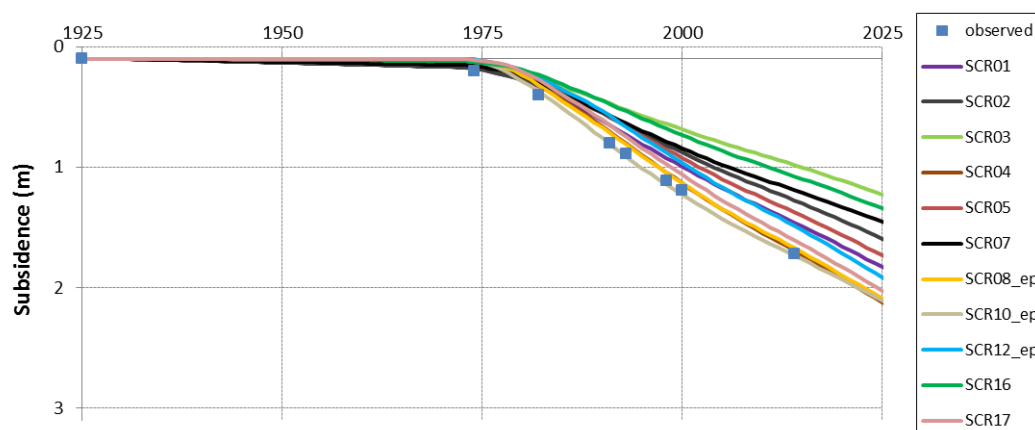

D.2.3 Optimized parameter values

The table shows the optimized OCR and POP values. Optimized Cv values can be inferred from the names shown in the graphs.

Scenario/model	RR	CR	Ca	OCR	POP (m)
SCR01	0.03	0.17	0.005	1.5	-
SCR02	0.03	0.15	0.005	1.6	-
SCR03	0.03	0.13	0.005	No fit	-
SCR04	0.03	0.17	0.002	1.2	-
SCR05	0.03	0.15	0.002	1.25	-
SCR06	0.03	0.13	0.002	No fit	-
SCR07	0.03	0.11	0.002	1.3	-
SCR08	0.03	0.17	0.000	**1.15**	-
SCR09	0.03	0.15	0.000	No fit	-
SCR10	0.03	0.13	0.000	No fit	-
SCR11	0.03	0.11	0.000	No fit	-
SCR12	0.03	0.17	0.000	-	**5**
SCR13	0.03	0.15	0.000	-	**3**
SCR14	0.03	0.13	0.000	-	**2**
SCR15	0.03	0.11	0.000	-	**2**
SCR16	0.02	0.11	0.002	No fit	-
SCR17	0.02	0.17	0.002	1.2	-

D.3 Marunda

D.3.1 Non-optimized subsidence to 2025.

D.3.2 Optimized parameter values

The table shows the optimized OCR and POP values. Optimized Cv values can be inferred from the names shown in the graphs.

| Scenario/model	RR	CR	Ca	OCR	POP (m)
SCR01	0.03	0.17	0.005	1.5	-
SCR02	0.03	0.15	0.005	1.6	-
SCR03	0.03	0.13	0.005	1.8	-
SCR04	0.03	0.17	0.002	1.2	-
SCR05	0.03	0.15	0.002	1.25	-
SCR06	0.03	0.13	0.002	No fit	-
SCR07	0.03	0.11	0.002	1.3	-
SCR08	0.03	0.17	0.000	**1.1**	-
SCR09	0.03	0.15	0.000	No fit	-
SCR10	0.03	0.13	0.000	**1.0**	-
SCR11	0.03	0.11	0.000	No fit	-
SCR12	0.03	0.17	0.000	-	**5**
SCR13	0.03	0.15	0.000	-	No fit
SCR14	0.03	0.13	0.000	-	**0**
SCR15	0.03	0.11	0.000	-	No fit
SCR16	0.02	0.11	0.002	1.3	-
SCR17	0.02	0.17	0.002	1.2	-

D.3.3 Modified drawdown for model SCR16_md

In this drawdown scenario that was used to obtain a fit for SCR16-md, 10 m extra drawdown develops early for the middle and deep depth levels and is maintained.
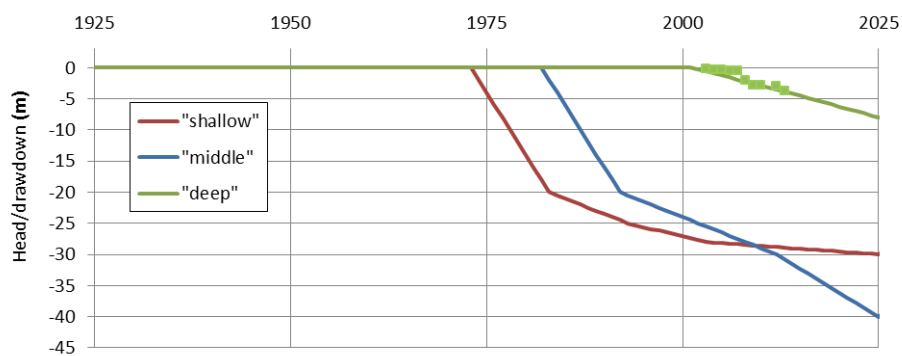

D.3.4 Intermediate rate recovery ($\tau = 30$ yr)

This scenario (3c) is based on a recovery rate that is intermediate relative to the slow (3a) and fast (3b) scenarios.
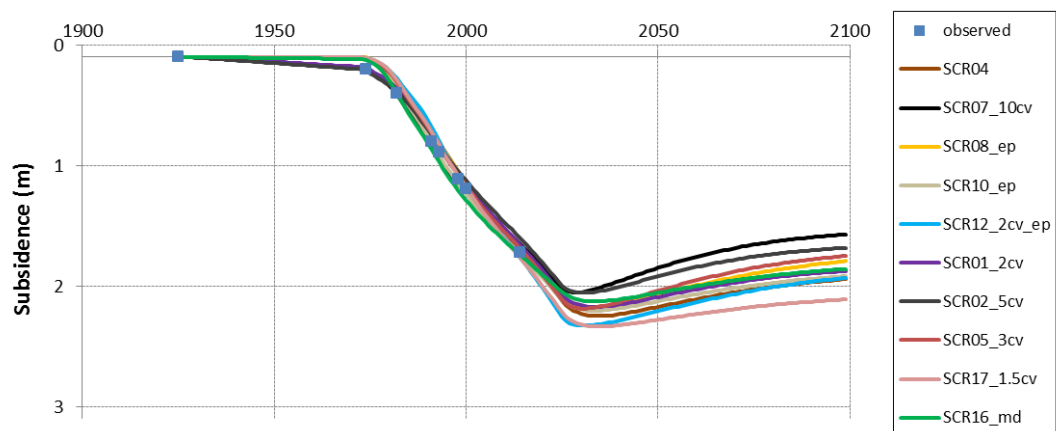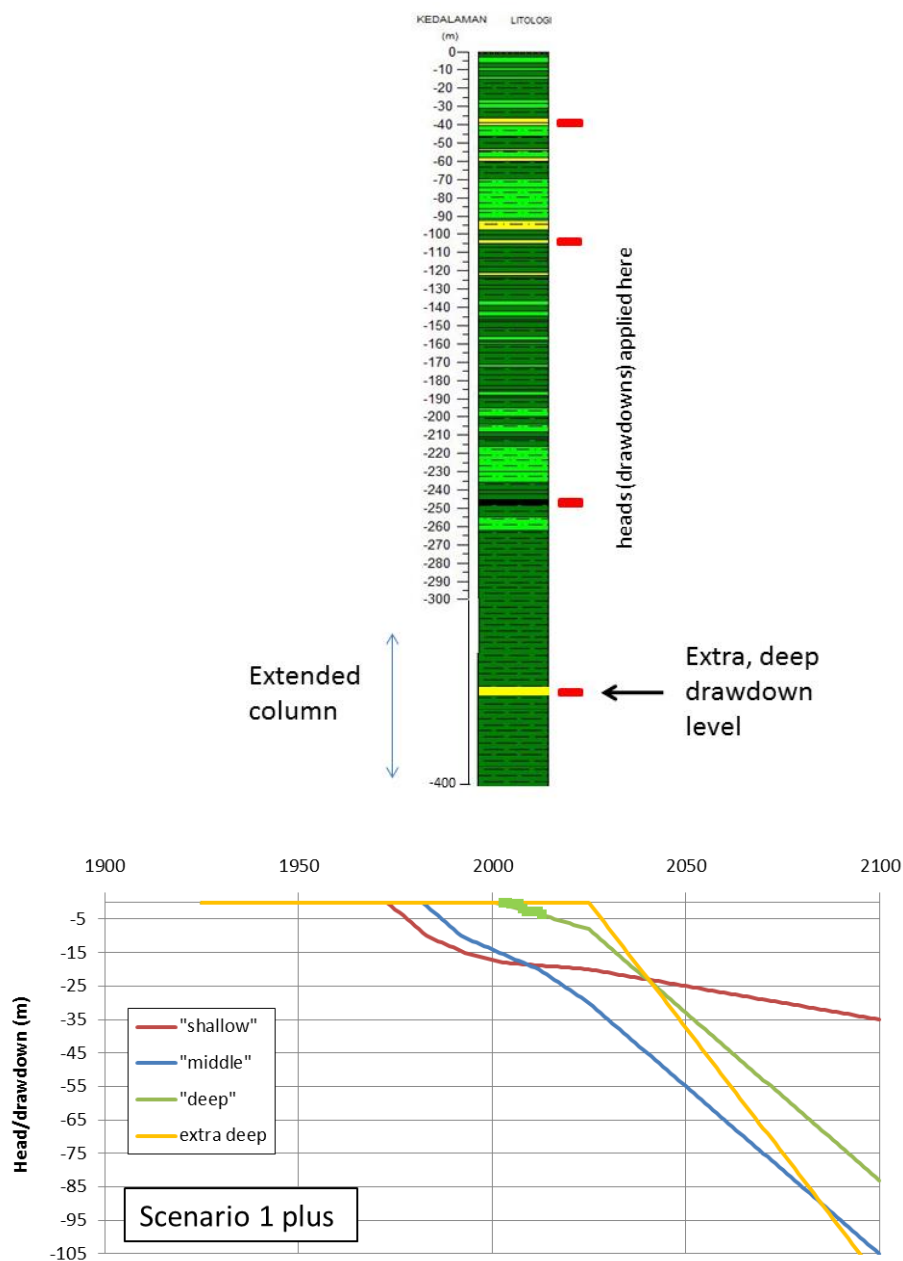
D.3.5 Head development for a selected model

These graphs illustrate the drawdown development for model SCR04 over the entire model depth section (borehole) for the stable head scenario (2) and for the intermediate rate recovery (3c) scenario. Subsidence for the latter scenario is shown in D.3.4. The strong delay in response of the low-permeability zones between the depths levels with imposed drawdown can be readily recognized.
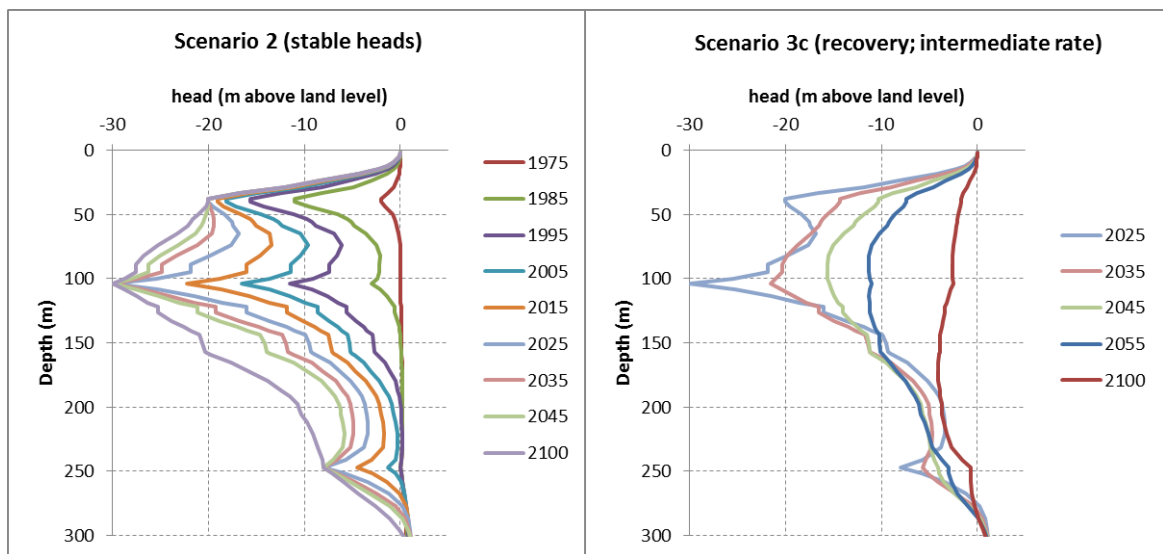
E   Business as usual 'plus' for Marunda

E.1   Extended model

The Marunda model domain is extended to 400 m depth with clay and a fictitiously sand layer at 350 m depth. At the sand layer 'extra deep' a fourth time series is applied in addition to those of scenario 1 in which drawdown increases 1.5 m/yr starting in 2025.

E.2   Subsidence